International Journal of Nanoelectronics and Materials
Volume 15 (Special Issue) December 2022 [59-70]

Design and Simulation of Optical Fibre Based of Gold Nanoparticles for Sensor Applications

Sara M. Tariq[1], and Makram A. Fakhri[1,*]

[1]Laser and Optoelectronic Engineering Department, University of Technology-Iraq, Baghdad, Iraq

ABSTRACT

In this study, we investigate an unclad single-mode fiber-optic biosensor by using COMSOL MULTIPHYSICS Finite Element Method (FEM) simulation. The key parameters of this study are the thickness and the refractive index (RI). The thickness of Au NPs was examined at 30nm, 40nm, and 50nm. Furthermore, the thickness of the analyte layer was also examined at 3μm, 4μm, and 5μm. This sensor was constructed using standard single-mode fiber. The cladding's middle section was removed, and gold nanoparticles (Au NPs) were deposited on it. It was found that at 50nm thickness of Au NPs, the confinement loss reached its maximum. Then, the Au NPs thickness was fixed at 50 nm and the analyte layer was changed. It was found that the confinement loss stayed nearly the same at the three thicknesses. The refractive index was also varied from 1.00027632 to 1.3403. After fixing the thickness of Au NPs and analyte layer at 50nm and 3μm, respectively, the sensitivity and resolution were measured and they were found to be 16129.03[nm/RIU] and 6.2×10-6[RIU], respectively, for colon tissue. This sensor provided theoretical analysis for experimental work. In addition to the simplicity of the design, this provides higher sensitivity.

Keywords: Gold nanoparticles, optical fiber sensor, biosensors, refractive index, Finite Element Method

1. INTRODUCTION

In recent years, food safety, environmental monitoring, drug development, clinical diagnosis, and biological research have all seen an increase in demand for fast, dependable, and extremely sensitive testing systems [1-4]. Because of their compact size, small footprints, low cost, quick response, and immunity to electromagnetic interference, fibre optic sensors are excellent choices for meeting the requirements [5-8].

Noble metal nanoparticles, particularly gold, have an important plasmonic effect when they come into contact with a dielectric material, and as a result, they have been widely used in the development of localized surface plasmon resonance (LSPR)-based sensors, in which they are immobilised on the surface of a fiber-optic [9-12]. This mechanism has been used to measure the refractive index variation in the media surrounding the probe, as well as for biological sensing when the nanoparticles are functionalized with antibodies, for example [13-16].

The localized electromagnetic field around metal surfaces is highly sensitive to the refractive index of the surrounding environment [17-19]. Changes in metal LSPR properties can be used to analyze environmental changes at media-metal interfaces [20-22]. The combination of sensors based on LSPR and optical fibres has several advantages [23, 24]. To begin, doubling the total reflection of light transmitted through an optical fiber stimulates a sample several times, potentially improving analyte detection sensitivity. Second, only 100-200 nm of the evanescent field penetrates the sidewall of an unclad fiber-optic [25-28].

*makram.a.fakhri@uotechnology.edu.iq, & mokaram_76@yahoo.com

As a result, the sensor is solely sensitive to environmental changes close to the optical fiber surface [29, 30]. Background noise can be reduced significantly in this manner [31, 32]. Finally, the optical fiber sensor based on the metal nanoparticle LSPR effect has a fast response, real-time detection, and is simple to adapt [33, 34]. The most common LSPR-based optical fiber sensor method involves removing a small section of the cladding from the center of the fiber-optic and coating the unclad portion with a monolayer of metal nanoparticles. The sensing medium surrounds the nanoparticle coated portion. [35-38]. The plasmon resonance of metal nanoparticles is excited by the evanescent field of light transmitted through the core of the fiber-optic [39, 40].

In 2010, H. Lee, et al. [41] a LSPR biosensor was fabricated by using standard fiber-optic which was etched in HF to remove a portion of the cladding. Gold nanoparticles (Au NPs) were used to coat the etched area of the fiber. The diameter and the surface density ratio of gold nanoparticles were varying to establish an optical fiber biosensor with optimized sensitivity. In 2015, R. Bharadwaj, et al. [42] it was demonstrated a U-bend fiber-optic biosensor with a core (200μm diameter) and a bend diameter (1.5mm). In this sensor, an immobilised Au NP was used to calculate plasmon penetration depth. The field of LSP was investigated using multi-layered nanostructures formed on immobilised Au NP. A polyelectrolyte multilayer shaped by layer-by-layer (LBL) deposition of oppositely charged polyelectrolytes was investigated, as was an immunoglobulin G (IgG) multilayer shaped by sequential immobilisation of two mutually specific antibodies. The LSPR biosensor's Plasmon penetration depth (d_p) was calculated by changing the analyte layer deposition with the LSPR absorbance measurement. When the plasmon field was probed with an IgG multilayer, the d_p was at least twofold higher than when the plasmon field was probed with a polyelectrolyte multilayer. The effect of Au NP size was also investigated, using Au NP with diameters of 18, 36, and 45 nm. The Au NP with a diameter of 36 nm had the highest d_p.

In 2020, D. I. Al-Janabi, et al. [43] for human temperature monitoring, an all-fiber, highly sensitive sensor -based gold nanoparticle-coated macrobent single mode fiber has been developed. SMF was bending to create a Mach-Zehnder model interferometer and construct the sensor by selecting the appropriate bending radius. By utilizing the magnetron sputtering technique, the Au NPs was coated over the sensing area of different bending SMFs with various tuned thicknesses of 10, 20 and 30-nm to experimentally examine the temperature-sensing performance. The best performance was showed by the sensor which coated by 20-nm Au NPs layer thickness with excellent sensitivity of −2.56 nm/°C, fast rise time of 1.73 ms and an excellent resolution of 1.82 $\times 10^{-4}$°C. The COMSOL Multiphysics FEM is sophisticated simulation software and widely utilized for scientific analyzing and research in various sectors [44-46]. The proposed sensor's sensing properties are investigated using the wave optics module in COMSOL Multiphysics. During the modelling process, the entire structure is separated into a small subdomain and enclosed by a perfectly matched layer (PML) barrier, which is used to absorb light radiated toward the surface [47-50].

In this study, we use COMSOL MULTIPHYSICS to simulate and model a fiber-optic biosensor. Single mode fiber SMF-28e of core (8.2 μm diameter) and cladding (125-μm diameter) is used [51, 52]. The middle portion of the cladding is removed and coated with AuNPs of different thicknesses (30, 40, and 50nm) at wavelength of 650 nm with different thicknesses of analyte layer of 3μm, 4μm, 5μm [53, 54]. In our work, the thickness was optimized, where it was found that 50nm thickness provided the best performance. Then, Au NPs thickness was fixed at 50nm and analytes thickness was changed, and it was found to be not affected the performance of the sensor. Because of the surface plasmon phenomenon between the core and the gold nanoparticle Au NP layer, the variation in the refractive index of the analytes affected the effective refractive index n_{eff}, makes the sensor highly sensitive to changes in the refractive index of the surrounding medium, as well as the effect of metal thickness on sensor performance. Furthermore, the

simplicity of sensor allows for sensing applications [57-60]. This sensor was created to improve sensitivity while also being simple to implement.

2. MODELING AND METHOD

At wavelength of 650nm, SMF-28e made of silica glass with (8.2μm) core diameter, (125.0± 0.7 μm) cladding diameter and (245±5 μm)coating diameter is employed. The coating was removed, then, the middle part of the cladding was removed. To provide the best confinement loss and enhance the sensitivity of the sensor, Au NPs with thicknesses of 30, 40, and 50 nm were deposited on the unclad portions, respectively.Then, the fiber is immersed in different liquids (water, lever tissue, and colon tissue) with different thicknesses of 3, 4, and 5 μm which equal 3000, 4000, and 5000 nm, after fixing the Au NPs thickness at 50nm. The COMSOL Multiphysics 5.1 simulation software, which is based on the FEM was used to simulate the sensor. Figure 1(a) and 1(b) show the geometry of the etched fiber and a cross section of the sensor, respectively.

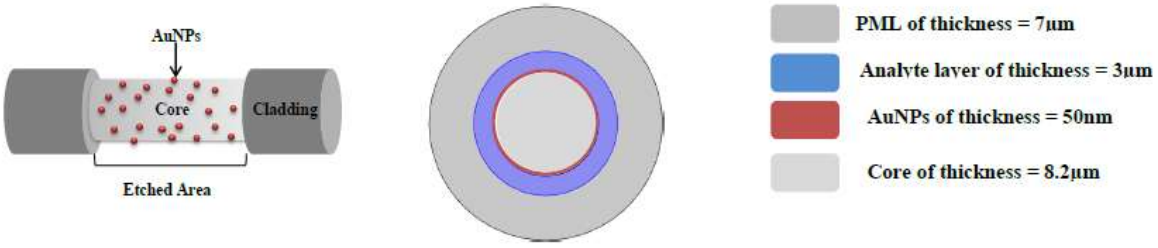

(a) (b)

Figure 1. Presents a) the geometry of etched fiber, and b) Cross section of the proposed sensor.

The silica glass whose index of refraction is calculated by Sellmeier equation [61]:

$$n^2(\lambda) = 1 + \frac{b_1 \lambda^2}{\lambda^2 - c_1} + \frac{b_2 \lambda^2}{\lambda^2 - c_2} + \frac{b_3 \lambda^2}{\lambda^2 - c_3} \quad (1)$$

Where n is the index of refraction, λ is the wavelength in the unit of μm, and b_1, b_2, b_3, c_1, c_2 and c_3 are the Sellmier equation constant. Those are taken from [62]. Table 1 shows the parameters of the proposed sensor designed by COMSOL.

Table 1 Psesents the parameters used to design the sensor by COMSOL

Name	Value	Discription
d_co	8.2[μm]	Core diameter
d_Au	8.25[μm]	Gold diameter
d_analyte	11.25[μm]	Analye diameter
PML	18.25[μm]	Perfectly matching layer
wl	650[nm]	Operating wavelength
fo	c_const/wl[nm]	Operating frequency
a1	0.696163	Sellmier coefficient
a2	0.4079426	Sellmier coefficient

a3	0.897479400	Sellmier coefficient
b1	$4.67914827\times10^{-3}[\mu m]^2$	Sellmier coefficient
b2	$1.35120621[\mu m]^2$	Sellmier coefficient
b3	$97.9240025[\mu m]^2$	Sellmier coefficient
n_s	Equation (1)	Sellmier equation
n_Au	0.29364	Gold refractive index
n_Air	1.00027632	Air refractive index

Table 2 shows the liquids used to fill the analyte layer and their refractive indices at 650-nm:

Table 2 The refractive indices of different liquids used as analytical materials at 650nm

The Biological Materials	The Refractive Index
Air (Empty Fiber)	1.00027632
Water	1.3310
Liver Tissue	1.3754
Colon tissue	1.3403

3. RESULTS AND DISCUSSION

The optical fibres have two components of light transmitted through them, the core's guided field and the cladding's evanescent field. This evanescent field decays exponentially along the cladding distance. As a result, the uniform fiber's use in sensing applications is unaffected because the light guided through the core cannot interact with the surrounding medium. As a result, we used an unclad fiber-optic configuration with an Au NP-coated core to LSPR and increase sensitivity [63-65].

In SPR phenomena, the free electron on the metal surface is excited by the evanescent field of the p-polarized wave, causing the surface Plasmon wave to propagate via the metal-dielectric interface. This is known as the resonance condition, and the wavelength is known as the resonance wavelength. The refractive index of the surrounding medium has a direct impact on the resonance wavelength. As the RI of the surrounding medium changes, the resonance wavelength also changes. As a result, we can simply determine the medium's RI by measuring this resonance wavelength [66-68].

The proposed sensor depends on its structure parameters. The key parameters of this sensor are the thickness of the Au NPs layer, the thickness of the analyte layer, and the refractive index. The thickness of the Au NPs has an important influence on the SPR performance, which should be considered first [69]. Thus, the thickness of the Au NPs layer was changed from 30 to 50nm in step of 10nm and the effect of SPR phenomenon was observed. The confinement loss of the sensor was determined for the three thicknesses by employing the effect of wavelength and the imaginary part $\mathrm{Im}(n_{eff})$ of n_{eff} of the core mode as shown in equation 2 [70-72]:

$$\alpha = 8.686 \times \frac{2\pi}{\lambda} \times \mathrm{Im}(n_{eff}) \times 10^9 \quad \left(\frac{\mathrm{dB}}{\mathrm{m}}\right) \tag{2}$$

Where λ is the wavelength of operation in a unit of nm.

Figure 3a, b, c, and d show the confinement loss curves at Au NPs thicknesses of 30, 40, and 50 nm for air (empty fiber), water, liver tissue, and colon tissue, respectively. It can be seen from this figure that confinement loss reached its maximum at a thickness of 50nm. The increase in the Au NPs layer thickness above 50nm can cause a higher damping loss, which causes decrease in the overall confinement loss of the fundamental mode. Furthermore, increasing the thickness above 50nm will cause decrease in the resonance depth as a result of the decay in the evanescent wave. As a result, a 50nm thickness was chosen to simulate the sensor by COMSOL Multyphysics 5.1.

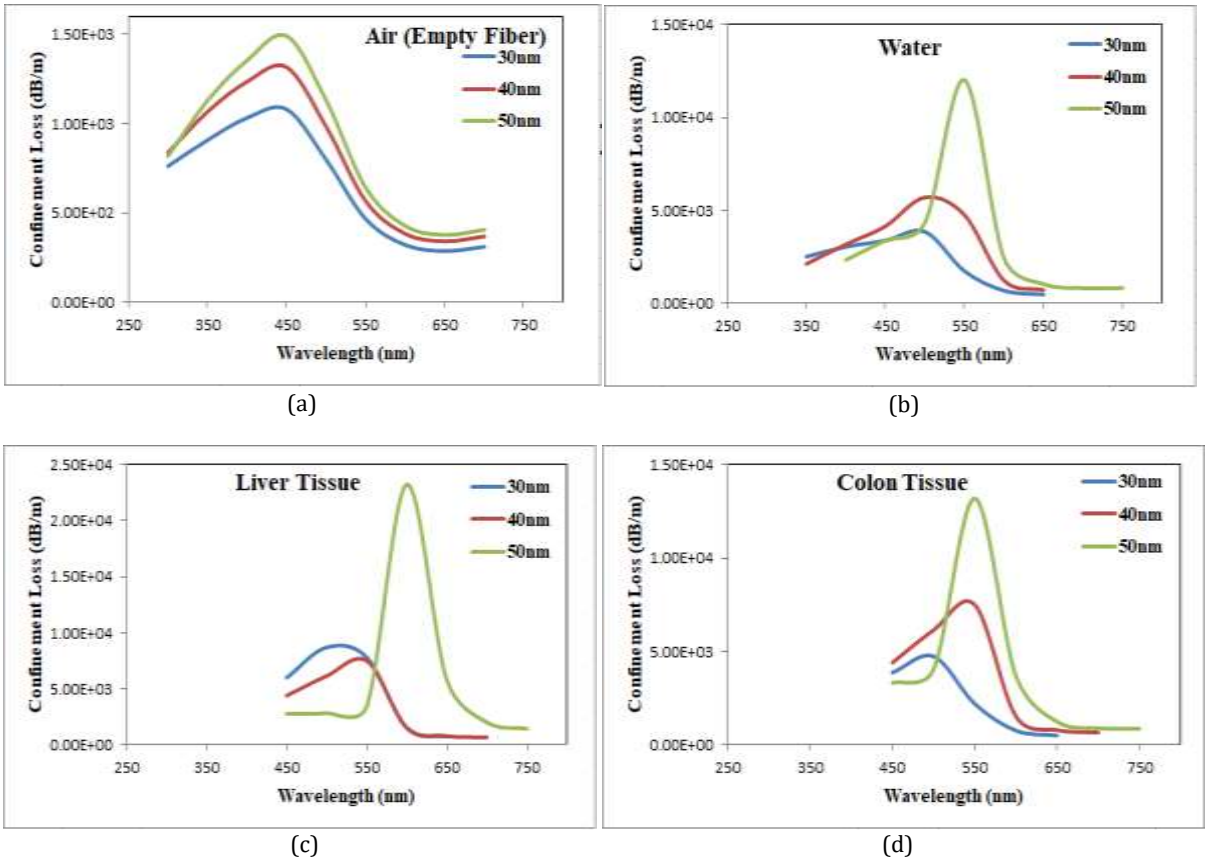

Figure 2. Presents the confinement loss (dB/m) of (a) Air (empty fiber), (b) water, (c) Liver tissue, and (d) Colon tissue, at AuNPs thickness of 30, 40, 50nm.

The RI of the surrounding environment is detected by the sensor. Thus, as the analyte layer RI changes, n_{eff} also changes. Furthermore, n_{eff} decreased as the wavelength increased. Figure 3 a, b, c, and d show the electric field distribution of the fundamental mode at which the electric field is confined in the core and the resonance mode at which most of the electric field is distributed around the Au NPs layer, for air (empty fiber), water, liver tissue, and colon tissue, respectively. The resonance mode takes place because of the coupling between the fundamental guided mode and the SPR mode. The wavelength at which the resonance mode appears is the resonance wavelength, where at this wavelength the fundamental guided mode and the resonance mode become nearly the same and the phase match condition is satisfied. Figure 3(a) shows the fundamental mode and the resonance mode for air. Despite the fact that the confinement loss reached its maximum for air at wavelength of 400 nm but the SPR condition is satisfied at700 nm, where n_{eff} of the two modes is 1.4538. Figure 3(b) shows the fundamental guided mode and resonance mode for water, where the SPR condition is satisfied at a wavelength of 550 nm with a n_{eff} of 1.459. Figure 3(c) shows the fundamental guided mode and resonance mode for liver tissue, where the SPR condition is satisfied at a wavelength of 600 nm with a n_{eff} of 1.4567. Figure 3(d) shows the fundamental mode and resonance mode for colon tissue, where the SPR condition is satisfied at a wavelength of 550nm with a n_{eff} 1.459.

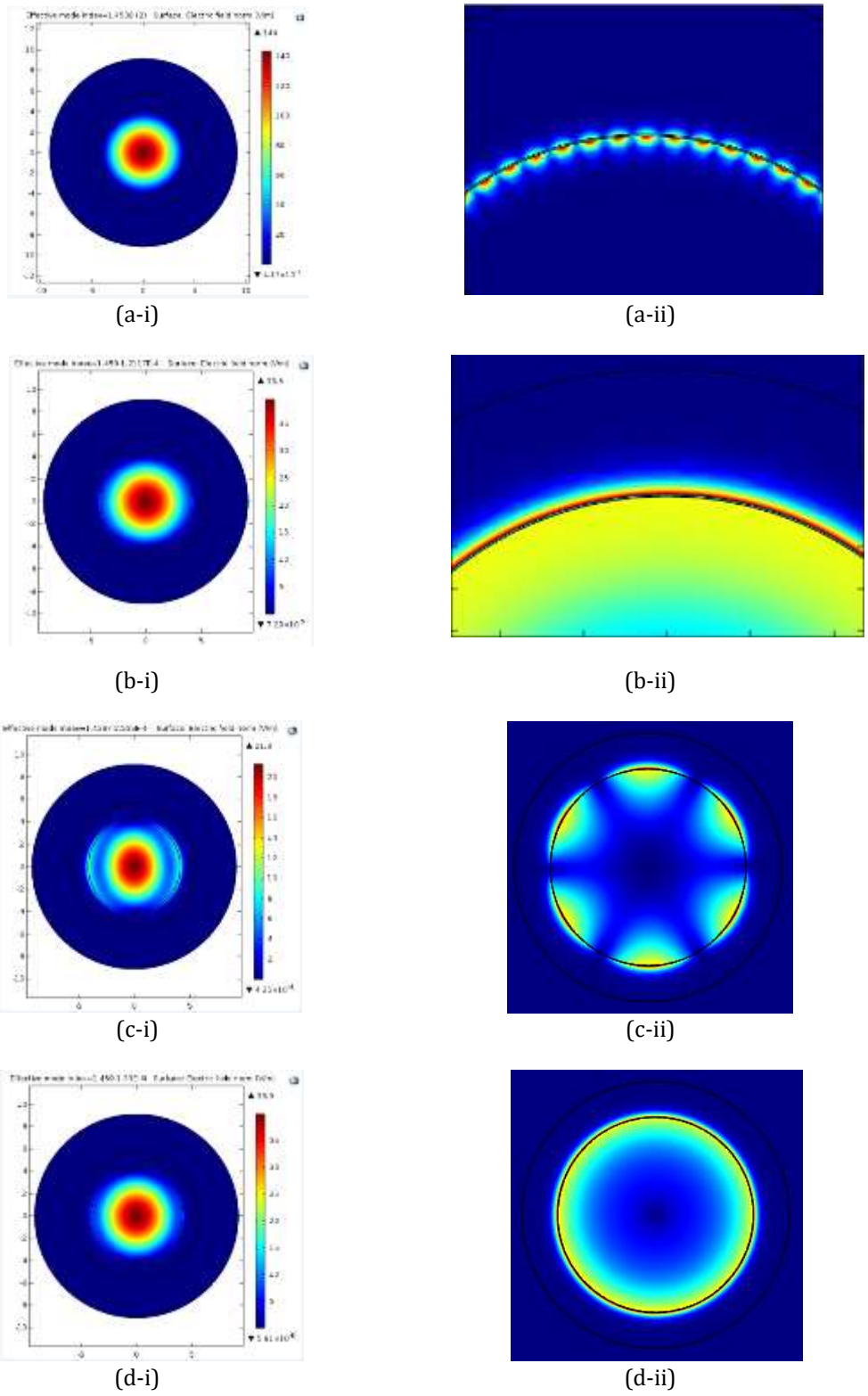

(a-i) (a-ii)

(b-i) (b-ii)

(c-i) (c-ii)

(d-i) (d-ii)

Figure 3. Presents shows the electric field dispersion spectrum of a-i) the fundamental core mode, and a-ii) The SPR mode, at 400nm for air (empty fiber), b-i) the fundamental core mode, and b-ii) The SPR mode, at 550nm for water, c-i) the fundamental core mode, and c-ii) The SPR mode, at 600nm for liver tissue, and of d-i) the fundamental core mode, and d-ii) The SPR mode, at 550nm for colon tissue.

The thickness of Au NPs was fixed at 50nm while the thickness of the analyte layer was varied from 3μm to 5μm in steps of 1μm (3000 to 5000) nm. The confinement loss in units of (dB/m) was determined for each thickness. Figure 4 a, b, c, and d show the confinement loss of air (empty fiber), water, liver tissue, and colon tissue, respectively, at analyte layer thickness of 3, 4, and 5μm. It can be observed that the confinement loss is nearly the same and varying the thickness does not affect it. As a result, 3μm thickness was chosen to the thickness of analyte layer.

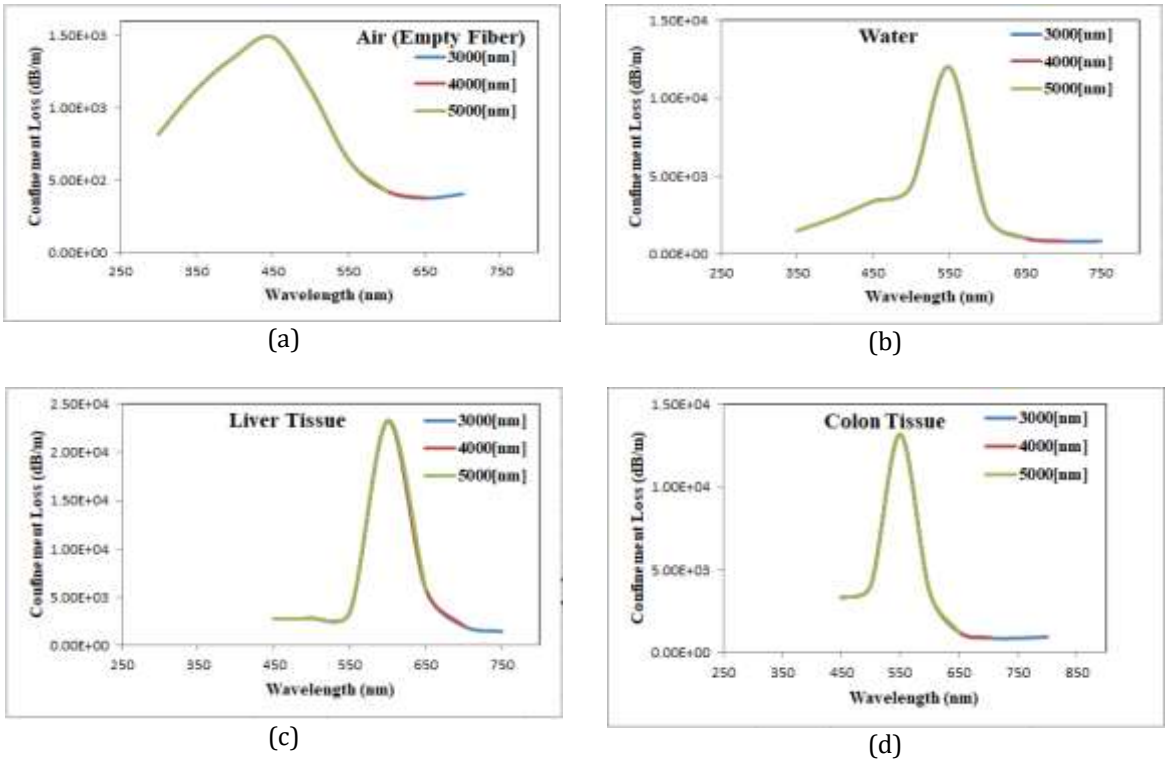

Figure 4. Presents the confinement loss (dB/m) of a) Air (empty fiber), b) Water, c) Liver tissue, and d) Colon tissue, at analyte layer thickness of 3000, 4000, and 5000nm.

As the thicknesses of Au NPs were fixed at 50nm and of the analyte layer at 3000nm, the amplitude sensitivity was determined. The amplitude sensitivity is indicated by $S_A(\lambda)$ and measured in units of $[RIU]^{-1}$. The S_A is given by equation (3) [73]:

$$S_A(\lambda)[RIU]^{-1} = \frac{1}{\alpha(\lambda,n_a)} \frac{\partial\alpha(\lambda,n_a)}{\partial n_a} \quad (3)$$

Where $\partial\alpha(\lambda, n_a)$ is the difference between two adjacent confinement losses caused by a small change in analyte RI. $\alpha(\lambda, n_a)$ is the overall confinement loss, and ∂n_a is the change of analyte RI. Figure 5 shows that the maximum amplitude sensitivities were 21.2252, 48.9302, 18.83182, and 13.2149 $[RIU]^{-1}$ for air (empty fiber), water, colon tissue, and liver tissue, respectively.

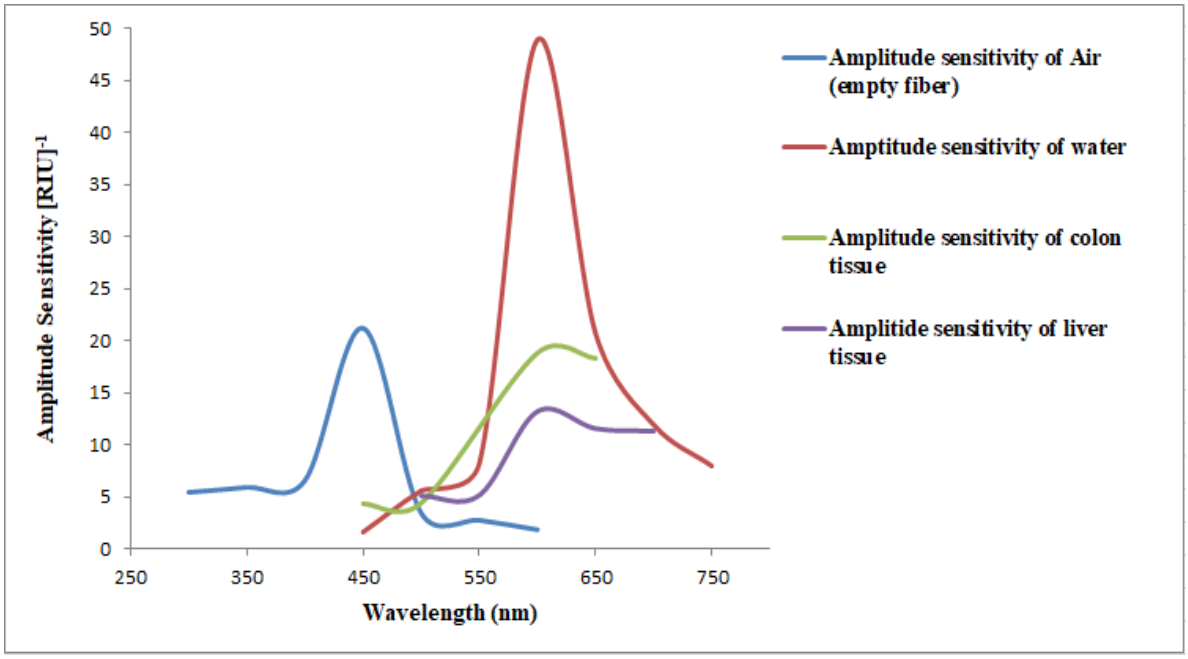

Figure 5. Presents the amplitude sensitivity in $[RIU]^{-1}$ for air, water, liver tissue, and colon tissue.

The second method that is used to measure the sensitivity is based on the variation in the refractive index that causes a variation in the resonance wavelength, influencing the sensitivity of the SPR sensor and is known as the wavelength sensitivity and is denoted by S_λ as shown in equation (4) [74]:

$$S_\lambda = \frac{\delta\lambda_{res}}{\delta n_s} \left[\frac{nm}{RIU}\right] \quad (4)$$

Where $\delta\lambda_{res}$ is the shift in resonant wavelength while δn_s is the shift in the analytes RI. The δn_s at 650nm were 1.331-1.000276, 1.3403- 1.331, and 1.3754-1.3403 which equal to 0.330724, 0.0093, and 2849.008. Whilst $\delta\lambda_{res}$ was equal to 150nm for water, colon tissue, and liver tissue. Thus, the calculated S_λ were 453.5508, 16129.03, and 4273.504 for water, colon tissue and liver tissue, respectively. It can be seen that the sensor shows the highest sensitivity for colon tissue. Thus, we can obviously see that the sensitivity of the sensor was optimized by optimizing the thickness of Au NPs.

Another important parameter is resolution, which describes the ability of the proposed device to detect small changes in analyte RI. It is given in equation (5) [44]:

$$R[RIU] = \frac{\Delta\lambda_{min}}{S_\lambda} \quad (5)$$

Where S_λ indicates the wavelength sensitivity while $\Delta\lambda_{min}$ indicates the minimum spectral resolution, which is equal to 0.1nm. It was found that the measured R[RIU] was 22×10^{-5}, 6.2×10^{-6}, and 2.34×10^{-5} [RIU] for water, colon tissue, and liver tissue, respectively. Table 3 compares our work to some previous works on different fiber-optic geometries.

Table 3 Presents a comparison between our work and different previous works

Geometry of the Fiber	Nanomaterial/ Film	Thickness	Refractive index range	Sensitivity	Ref.
Etched Plastic Optical Fiber(POF)	Thin Au film	55nm	1.3353–1.3653	1600 nm/RIU	[75]
Dual D-shape photonic crystal fibers (PCFs)	Ag layer	50nm	1.36-1.41	14660 nm/RIU	[76]
Tilted fiber Bragg gratings (TFBGs)	Au layer	35 nm	1.34-1.37	124.89 nm/RIU	[77]
D-shaped	Ag layer	40 nm	1.333–1.345	2166 nm/RIU	[78]
Double-sided polished fiber	Au film	50 nm	1.42.	4284.8 nm/RIU	[79]
This work	Au NPs	50 nm	1.3310-1.3754	16129.03 nm/RIU	-

4. CONCLUSSION

In this work, unclad fiber-Optic sensor was designed by employing single mode fiber SMF-28e and AuNPs. AuNPs was deposited on the unclad portion of the fiber to offer enhancement sensitivity. First, the AuNPs thickness was optimized, where 30, 40, and 50nm thicknesses of AuNPs was deposited respectively on the core. It was found that a 50nm thickness provided the best performances. Second, the AuNPs thickness was fixed at 50nm and the thickness of the analyte layer was changed from 3μm to 5μm in steps of 1μm (3000 to 5000) nm. It was found that the analyte thickness does not affect the performance of the sensor. As a result, 3μm analyte thickness was chosen to fill with different liquids (water, colon tissue, and liver tissue). The RI was changed from 1.3310-1.3754. The sensitivity and resolution of the sensor for the three liquids were measured, and it was found to have the best results for colon tissue. The wavelength sensitivity of the colon tissue was 16129.03nm/RIU while the resolution was 6.2×10^{-6} [RIU]. The proposed sensor provides a theoretical basis for testing.

ACKNOWLEDGEMENTS

The authors thank Laser and Optoelectronic Department, University of Technology-Iraq, Baghdad, Iraq for the logistic support this work.

REFERENCES

[1] Li, K., Zhou, W., Zeng, S., 2018. Sensors. 18, 3295.
[2] Su, H., Li, S., Jin, Y., Xian, Z., Yang, D., Zhou, W., Mangaran, F., Leung, F., Sithamparanathan, G., Kerman, K., 2017. Dovepress. 3, 19–29.
[3] Tawfiq, Z.H., Fakhri, M.A., Adnan, S.A., 2018. IOP Conf. Series: Materials Science and Engineering. 454 (Issue 1), 012173.
[4] Awayiz, M.T., Salim, E.T., 2020. Materials Science Forum. 1002, 200-210.
[5] Mavrogiannis, N., Crivellari, F., Gagnon, Z.R., 2016. Biosens Bioelectron. 77, 790–798.
[6] Chau, L., Lin, Y., Cheng, S., and Lin, T., 2006. Sensors and Actuators B: Chemical. 113, 100–105.
[7] Ali, H.S., Fakhri, M.A., Khalifa, Z., 2021. Journal of Physics: Conference Series. 1795 (Issue 1), 012065.

[8] Faisal, A.D., Ismail, R,A., Khalef, W,K., Salim, E.T., 2020. Optical and Quantum Electronics. 52, 1-12.
[9] Wang, X.D., Wolfbeis, O.S., 2016. Anal. Chem. 88,203–227.
[10] LC. Jr. Clark, R. Wolf, D. Granger, Z. Taylor, 1953. Continuous recording of blood oxygen tensions by polarography, J Appl Physiol. 6 (Issue 3), 189–193.
[11] Ali, H.S., Fakhri, M.A., 2020. Materials Science Forum. 1002, 282-289.
[12] Salim, E.T., Ismail, R.A., Halbos, H.T., 2019. Materials Research Express. 6 (Issue 11), 116429.
[13] Guerreiro, J.R.L., Frederiksen, M., Bochenkov, V.E., Freitas, V., Sales, M.G.F., and Sutherland, D.S., 2014. ACS Nano. 8, 7958–7967.
[14] Wang, J., 2008. Chem Rev. 108, (Issue 2), 814–825.
[15] Jabbar, H.D., Fakhri, M.A., Abdulrazzaq, M.J., 2021. Materials Today: Proceedings. 42 (Issue 5), 2829-2834.
[16] Awayiz, M.T., Salim, E.T., 2020. AIP Conference Proceedings. 2213 (Issue 1), 020247.
[17] Tu, M.H., Sun, T., Grattan, K.T.V., 2014. Sensors and Actuators B. 191, 37– 44.
[18] Taylor, R., Sylvain, C., Todd, O., 2013. J. Appl. Phys. 113 (Issue 1) 011301.
[19] Fakhri, M.A., Tawfiq, Z.H., Adnan, S.A., 2020. AIP Conference Proceedings. 2213 (Issue 1), 020245.
[20] Asady, H., Salim, E.T., Ismail, R.A., 2020. AIP Conference Proceedings. 2213 (Issue 1), 020183.
[21] Wang, Z., Hou, R., Zheng, Z., Zhu, 2013. J., Nanosci. J., Nanotechnol. 13, 1476.
[22] Huong, V.T., Phuong, N.T.T., Tai, N.T., An, N.T., Lam, V.D., Manh, D.H., Chi, T.T.K., Mai, N.X.D., Phung, V.D., Tran, N.H.T., 2021. Journal of Nanomaterials. 2021, Article ID 5530709.
[23] Adnan, S.A., Tawfiq, Z.H., Fakhri, M.A., 2020. Defect and Diffusion Forum. 398, 23-28.
[24] Abood, M., Salim, E.T., Saimon, J.A., 2019. Journal of Ovonic Research. 15 (Issue 2), 109–115.
[25] Shao, Y., Xu, S., Zheng, X., Wang, Y., Xu, W., 2010. Sensors. 10, 3585-3596.
[26] Zeng, S., Yong, K., Roy, I., Dinh, X.-Q., Yu, X., and Luan, F., 2011. Plasmonics. 6, 491–506.
[27] Hassan, N.K., Fakhri, M.A., Salim, E.T., Hassan, M.A., 2021. Materials Today: Proceedings. 42, 2769-2772.
[28] Alsultany, F.H., Alhasan, S.F.H. & Salim, E.T., 2021. J Inorg Organomet Polym. 31, 3749–3759.
[29] Wang, Y., Zhou, J., and Li, J., 2017. Small Methods. 1, 1700197.
[30] Jain, P.K., Lee, K.S., El-sayed, I H., and El-sayed, M.A., 2006. Journal of Physical Chemistry B. 110, 7238–7248.
[31] Husam, A.A.A, Fakhri, M.A. Alwahib, A.A., 2021. Materials Today: Proceedings. 42, 2815-2821.
[32] Ismail, R.A., Salim, E.T., Halbos, H T., 2021. Optik. 245, 167778.
[33] Srivastava, S.K., Gupta, B.D., 2013. The Open Optics Journal. 7, 58-83.
[34] Saha, K., Agasti, S., Kim, C., Li, X., and Rotello, V.M., 2012. Chemical Reviews. 112, 2739–2779.
[35] Hassan, M.A., Al-Nedawe, B.M., Fakhri, M.A., 2021. Applied Optics. 60 (Issue 8), 2339-2347.
[36] Alghurabi, M.N.A.K., Mahmood, R.S., Salim, E.T., Alhasan, S.F.H., Khalid, F.G., 2021. Materials Today: Proceedings. 42, 2497-2501.
[37] Willets, K.A., and Duyne, R.P.V., 2007. Annual Review of Physical Chemistry. 58, 267–297.
[38] Do, P.Q.T., Huong, V.T., Phuong, N.T.T., 2020. RSC Advances. 10, 30858–30869.
[39] Hassan, M.M., Fakhri, M.A., Adnan, S.A., 2019. Digest Journal of Nanomaterials and Biostructures. 14 (Issue 4), 873-878.
[40] Salim, E.T., Ismail, R.A., & Halbos, H.T., 2020. Appl. Phys. A. 126, 891.
[41] Lee, H., Kim, H.-J., Park, J.-H., Jeong, D. H., Lee, S.-K., 2010. Measurement Science and Technology. 21 (Issue 8), 085805.
[42] Bharadwaj, R., Mukherji, S., Mukherji, 2015. Plasmonics. 11 (Issue 3), 753-761.

[43] Al-Janabi, D.I., Salman, A.M., Al-Janabi, A., 2020. Journal of Nanophotonics. 14 (Issue 4), 046013-1.
[44] Gangwar, R.K., Min, R., Kumar, Li, X., 2021. Frontiers in Physics. 9, 707113.
[45] Unser, S., Bruzas, I., He, J., and Sagle, L., 2015. Sensors. 15, 15684–15716.
[46] Lu, M., Zhu, H., Bazuin, C.G., Peng, W., and Masson, J.F., 2019. ACS Sensors. 4, 613–622.
[47] Salim, E.T., Saimon, J.A., Abood, M.K., Fakhri, M.A, 2020. Optical and Quantum Electronics. 52 (Issue 10), 463.
[48] Jeong, H., Erdene, N., Park, J., Jeong, D., Lee, H., and Lee, S., 2013. Biosensors and Bioelectronics. 39, 346–351.
[49] Vidotti, M., Carvalhal, R.F., Mendes, R.K., Ferreira, D.C.M., Kubota, L.T., 2011. J. Braz. Chem. Soc. 22, 3-20.
[50] Mahdi, R.O., Fakhri, M.A., Salim, E.T., 2020. Materials Science Forum. 1002, 211-220.
[51] Thévenot, D.R., Toth, K., Durst, R.A., Wilson, G.S., 2001. Biosens and Bioelectron. 16, 121.
[52] Fen, Y.W., Yunus, W.M.M., Yusof, N.A., 2012. Sensors and Actuators B. 171–172, 287–293.
[53] Fakhri, M.A., Salim, E.T., Abdulwahhab, A.W., Hashim, U., Minshid, M.A., Salim, Z.T., 2019. Surface Review and Letters. 26 (Issue 10), 1950068.
[54] Aragoni, M.C., Area, M., Demartin, F., Devillanova, F.A., Isaia, F., Garau, A., Lippolis, V., Jalali, F. Papke, U., Shamsipur, M., Tei, L., Yari, A., Verani, G., 2002. Inorg. Chem. 41, 6623–6643.
[55] Zhang, X.B., Guo, C.C., Li, Z.Z., Shen, G L., Yu, R.Q., Anal. Chem. 74, 821–825.
[56] Salim, E.T., Fakhri, M.A., Tareq, Z.T., Hashim, U., 2020. AIP Conference Proceedings. 2213, (Issue 1), 020230.
[57] Kim, Y., Johnson, R.C., Hupp, J.T., 2001. Nano Lett. 1, 165–167.
[58] Li, C., Li, Z., Li, S., Zhang, Y., Sun, B., Yu, Y., Ren, H., Jiang, S., Yuei, W., 2020. Optics Express. 28, 6071.
[59] Fakhri, M.A., Abdul Razzaq, M.J., Alwahib, A.A., Muttlak, W.H., 2020. Optical Materials. 109, 110363.
[60] Shao, Y., Xu, S., Zheng, X., Wang, Y., and Xu, W., 2010. Sensors. 10 (Issue 4), 3585–3596.
[61] Hassan, MD.N. MD.W. and Rahman, Md. T., 2021. OSA Continuum. 4, 2615-2629.
[62] Anik, M.H.K., Isti, M.I.A., Islam, S.M.R., Mahmud, S., Talukder, H., Piran, M.J., Biswas, S.K., and Kwak, K.S., 2021. IEEE Access. 9, 2924–2933.
[63] Lin, Y., Zou, Y., Mo, Y., Guo, J., Lindquist, R. G., 2010. Sensors. 10 (Issue 10), 9397–9406.
[64] Mohsin, M.H., Numan, N.H., Salim, E.T., Fakhri, M.A., 2021. Journal of Renewable Materials. 9 (Issue 9), 1519-1530.
[65] Ghodselahi, T., Neishaboorynejad, T., Arsalani, S., 2015. Appl. Surf. Sci. 343, 194–201.
[66] Cao, J., Tu, M.H., Sun, T., Grattan, K.T.V., 2013. Sens. Actuators, B. 181, 611–619.
[67] Salim, E.T., Khalid, F.G., Fakhri, M.A., Mahmood, R.S., 2021. Materials Today: Proceedings. 42, 2422-2425.
[68] Haes, A.J., A.J. Duyne, A.J., 2004. Anal. Bioanal. Chem. 379 (Issue 7-8), 920–930.
[69] Jatschka, J., Dathe, A., Csáki, A., Fritzsche, W., Stranik, O., 2016. Sens. Biosensing Res. 7, 62–70.
[70] Rifat, A.A., Mahdiraji, G.A., Ahmed, R., Chow, D.M., Sua, Y.M., Shee, Y.G., and Adikan, F.R.M., 2017. IEEE Photonic Journal. 8 (Issue 1), 1-8.
[71] Du, Y., and Dong, S., 2017. Anal Chem. 215, 189.
[72] Gui, Q., Lawson, T., Shan, S., Yan, L., and Liu, Y., 2017. Sensors. 17, 1623.
[73] Liu, C., Wang, F., Lv, J., Sun, T., Liu, Q., Mu, H., and Chu, P. K., 2015. Journal of Nanophotonics. 9 (Issue 1), 093050.
[74] Zakaria, R., Zainuddin, N.A.M., Raya, S.A., Alwi, S.A.K., Anwar, T., Sarlan, A., Ahmed, K., and Amiri, I.S., 2020. Micromachines. 11 (Issue), 77.
[75] Al-Qazwini, Y., Noor, A.S.M., Al-Qazwinic, Z., Yaacob, M.H., Harun, S.W., M.A. Mahdi, 2016. Sensors and Actuators A. 246, 163-169.
[76] Liu, C., Su, W., Liu, Q., Lu, X., Wang, F., Sun, T., and Chu, P.K., 2018. Optics Express. 26 (Issue 7), 9039-9049.
[77] Lobry, M., Loyez, M., Hassan, E.M., Chah, K., Derosa Derosa, M.C., Goormaghtigh, E., Wattiez, R., and Caucheteur, C., 2020. Optics Express. 28, 7593-7551.

[78] Zainuddin, N.A.M., Ariannejad, M.M., Arasu, P.T., Harun, S.W., and Zakaria, R., 2019. Results in Physics. 13, 102255.
[79] Liu, L., Deng, S., Zheng, J., Yuan, L., Deng, H., and Teng, C., 2021. Sensors. 21 (Issue 4), 1516.